J Mater Sci (2007) 42:4692–4700
DOI 10.1007/s10853-006-0347-6

Experimental investigation on constitutive behaviour of superconducting powder BSCCO

Yinghong Zhao · Pan Zeng · Liping Lei · Hanping Yi

Received: 4 January 2006 / Accepted: 17 April 2006 / Published online: 31 January 2007

Abstract As a superconducting material, Bi 2233/Ag tape needs high-critical transport current density J_c, which is influenced by the uniform deformation and density of BSCCO powder in filaments during the forming process. The aim of this paper is to investigate the constitutive behaviour of BSCCO powder. The modified Drucker–Prager/Cap model is introduced to describe the constitutive behaviour of BSCCO powder. A series of cyclic loading experiments for BSCCO powder in a cylinder die were carried out. Based on the experiments, the relationships between the radial stress and the axial stress were obtained, and the parameters in the constitutive model were calculated. By pushing the compact powder from the die, the coefficient of friction between the BSCCO powder and the cylinder die was determined. Finally, the modified Drucker–Prager/Cap model is proposed and used to simulate the confined compression test of BSCCO powder.

Y. Zhao (✉) · P. Zeng · L. Lei
Department of Mechanical Engineering,
Tsinghua University, Beijing 100084, P.R. China
e-mail: zhaoyh03@mails.tsinghua.edu.cn

Y. Zhao · P. Zeng · L. Lei
Key Laboratory for Advanced Materials Processing Technology, Ministry of Education, Beijing 100084, P.R. China

H. Yi
Innova Superconductor Technology Co. Ltd., 7 Rongchang Dongjie, Longsheng Industrial Park, Beijing 100176, P.R. China

Introduction

The oxide powder in tube (OPIT) technique for manufacturing high-temperature Bi-2223/Ag superconductor involves multi-step drawing and roll processing. A pure silver tube is filled with isostatically compressed bars of BSCCO powder (the compressed relative density was about 40%, and the theoretical full density of BSCCO-2212 was 6.45 g/cm^3), the shape of BSCCO powder is plate-like, as shown in Fig. 1. After being drawn into a round wire 2 mm in diameter, the relative density of BSCCO powder increases to about 60% and the filament is cut into monofilaments, which are re-packed into a silver alloy tube with a diameter of 10 mm. The composite is subjected to the same drawing process to a final diameter of 1.5 mm. Thereafter the wire is rolled to a flat tape, 0.25 mm in thickness and 4 mm in width. Subsequently heat treatment is needed to sinter the powder, and the BSCCO-2223 phase is created [1].

The uniform deformation and high relative density of BSCCO powder in filaments play important roles in achieving a high critical transport current density J_c. The compressed deformation of BSCCO powder in OPIT is a complicated process involving large deformation, large strain and non-linear material behaviour. It is difficult to determine the proper design for the forming process. Recently, numerical simulation has been widely applied in ceramic powder forming. However, an improper material constitutive model can lead to unsuccessful simulations, and even erroneous conclusions. The aim of the present work is to investigate the constitutive behaviour of superconducting ceramic powder by cycle loading experiments.

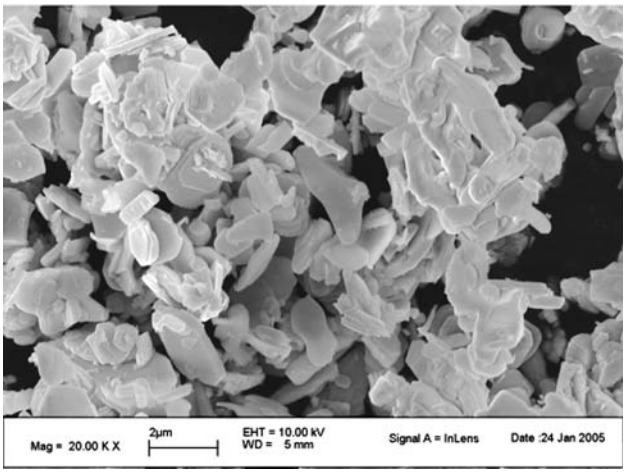

Fig. 1 SEM photographs of BSCCO powder

A variety of constitutive models of powder are currently available and they may be roughly classified into two groups: microscopic models and macroscopic models [2]. Microscopic models are known as direct models [3–6], which consider the discrete nature of the powder particles. Its framework encompasses the local behaviours between the particles such as particle contact, sliding, crushing, rolling and segregation. These models fail to model real complex situations like the particles collapsing during the process or the shape irregularity of local dislocations. Moreover, these simulations require great amounts of computation time, because many particles have to be taken into account. Macroscopic models [7–9] idealize the aggregation of the powder as an equivalent continuum material. A common characteristic of these models is the use of the plasticity theory. Unlike the continuum material, the yielding of powder material is caused by not only the deviatoric stress but also the hydrostatic stress. Therefore the yield criterion of powder material should be a function of both the first and second invariant of the deviatoric stress tensor. Both approaches have advantages and disadvantages in the modelling of powder material compaction. Nonetheless, from an industrial viewpoint, macroscopic models have a definitive edge over microscopic models in that the gross behaviour of the powder mass can be modelled and simulated on an industrial scale.

The particle size of BSCCO precursor is so small that it can be considered as a continuous medium during the forming process. In order to determine a suitable constitutive model for BSCCO powder, some experiments were performed [10–12].

Gurson and Yuan [10] studied the constitutive behaviour with a focus on experiments to obtain the Young's modulus, Poisson's ratio and hydrostatic stress with density and yield cap plasticity. Bech et al. [11] constructed the simplest constitutive plasticity model of Drucker–Prager/Cap, which does not have a horizontal tangent allowing for plastic strain without hardening and volumetric strain. Allais et al. [12] studied a simplified compressible model of the CAM-CLAY type with work hardening and softening depending on density variation. These experiments in the works mentioned above have some disadvantages because the expensive equipment and complex set-up, to some extent, prevent them from being used as regular approaches. In this paper, a systematic method for studying the constitutive model of BSCCO powder under a series of simple confined compression experiments was presented. The paper also described the use of modified Drucker–Prager/Cap elastic-plasticity model and evaluation of the parameters of this model for BSCCO powder based on experiments.

Description of constitutive behaviour of BSCCO powder

In this study, the modified Drucker–Prager/Cap elastic-plasticity model, as shown in Fig. 2, was adopted to model the constitutive behaviour of BSCCO powder. In this continuum model, the BSCCO powder is considered as a macroscopically porous medium and is characterized by overall density-dependent parameters, such as the cohesion, the global interparticle friction and the mechanical properties of particles. Moreover, with the increase of compressive load, the mechanical stress evolves in a bounded domain according to the plastic hardening mechanism.

The modified Drucker–Prager/Cap model, having a multi-yield surface, enables the effects of the stress state to be addressed during compression mode. The yield surface has two principal segments: a pressure-dependent modified Drucker–Prager shear failure

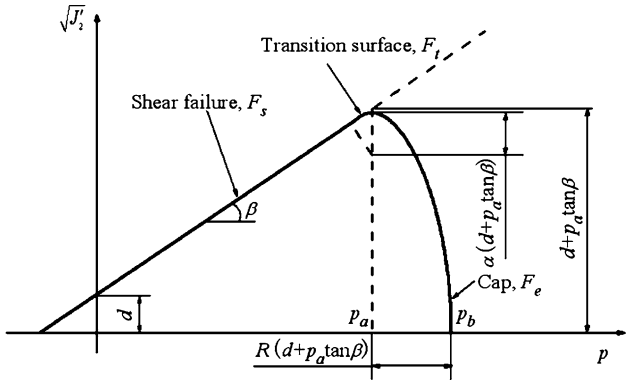

Fig. 2 Modified Drucker–Prager/Cap model in $p-\sqrt{J_2'}$ plane

segment and a compression cap segment. The modified Drucker–Prager failure segment is a perfectly plastic yield surface (no hardening). Plastic flow on this segment produces inelastic volume increase (dilation) that causes the cap to soften. On the cap surface, plastic flow causes the material to compact. There is a transition region between these segments, introduced to provide a smooth surface, where

$$p = (\sigma_1 + \sigma_2 + \sigma_3)/3 \tag{1}$$

and

$$\sqrt{J_2'} = \sqrt{\frac{1}{6}[(\sigma_1 - \sigma_2)^2 + (\sigma_2 - \sigma_3)^2 + (\sigma_3 - \sigma_1)^2]} \tag{2}$$

Stress–strain relationship

In the elastic–plastic model, the total strain increment tensor includes the elastic strain increment $d\varepsilon^{\mathrm{el}}$ and the inelastic strain increment $d\varepsilon^{\mathrm{pl}}$. The elastic behaviour is assumed to be linear:

$$d\varepsilon_{ij}^{\mathrm{el}} = \frac{1+v}{E} d\sigma_{ij} - \frac{v}{E} d\sigma_{kk}\delta_{ij} \tag{3}$$

where E and v are the Young's modulus and Poisson's ratio, which depend on the local density during compression. In this paper, the calibration of the elastic parameters of E and v is described in Sect. 4.

Multi-yield surfaces

The shear failure yield surface [13, 14], F_{s}, is a criterion to characterize the shear stress required for simple slip depending on the cohesion and the hydrostatic pressure p:

$$F_{\mathrm{s}} = \sqrt{J_2'} - p\tan\beta - d = 0 \tag{4}$$

where β is the internal angle of friction and d is the cohesion of granular material.

The cap yield surface [13, 14], F_{c}, has an elliptical shape with a constant eccentricity R. This cap can expand or contract as the inelastic volumetric strain decreases or increases, respectively. The cap equation is given by

$$F_{\mathrm{c}} = \left\{ (p - p_{\mathrm{a}})^2 + \left(\frac{R\sqrt{J_2'}}{1 + \alpha - \alpha/\cos\beta} \right)^2 \right\}^{1/2} - R(d + p_{\mathrm{a}}\tan\beta) = 0 \tag{5}$$

where R is eccentricity, which controls the shape of the cap, α is a small number (typically 0.01–0.05) for a smoothed transition yield surface from F_{c} to F_{s} and p_{a} is the evolution parameter, which is related to the hydrostatic compression yield stress p_{b} as follows:

$$p_{\mathrm{a}} = \frac{p_{\mathrm{b}} - Rd}{1 + R\tan\beta} \tag{6}$$

The hydrostatic compression yield stress p_{b} controlling the position of the cap, shown in Fig. 2, is an increasing function of the corresponding volumetric plastic strain $\varepsilon_{\mathrm{vol}}^{\mathrm{pl}}$, as shown in Fig. 3.

The transition yield surface F_{t} that connects F_{c} and F_{s} surfaces into a smooth one and avoids the corner problem for numerical computation is as follows:

$$F_{\mathrm{t}} = \left\{ (p - p_{\mathrm{a}})^2 + \left[\sqrt{J_2'} - \left(1 - \frac{\alpha}{\cos\beta} \right) \times (d + p_{\mathrm{a}}\tan\beta) \right]^2 \right\}^{1/2} - \alpha(d + p_{\mathrm{a}}\tan\beta) = 0 \tag{7}$$

Evolution equation

The volumetric plastic strain $\varepsilon_{\mathrm{vol}}^{\mathrm{pl}}$ is the trace of the plastic strain tensor $\varepsilon^{\mathrm{pl}}$[15]. Its variation directly affects the actual aggregate density ρ as follows:

$$\rho = \rho_0 \mathrm{e}^{-\varepsilon_{\mathrm{vol}}^{\mathrm{pl}}}, \tag{8}$$

where $\varepsilon_{\mathrm{vol}}^{\mathrm{pl}}$ is the volumetric plastic strain, and ρ_0 is the initial loose state density.

Compression experiments of BSCCO powder

At present, there are two main methods, i.e., ultrasound wave method [10] and mechanical testing

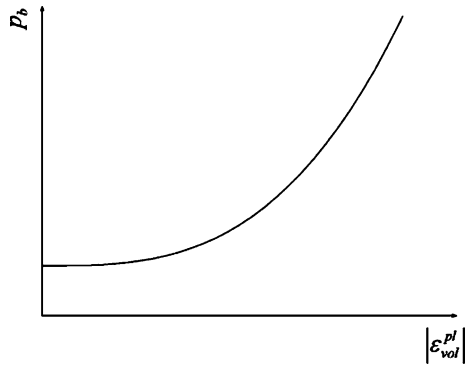

Fig. 3 Cap hardening

method [11], to study the constitutive behaviour of powder aggregates. In this work, the mechanical testing method was adopted, and confined compression experiments were needed.

The confined compression experiments were performed on loose powder samples contained in a cylindrical die with a strain gauge on the outside wall of the die, as shown in Fig. 4a. The larger the range of pressure measured is, the thicker the wall of the die must be. But, a thicker die wall can result in low accuracy of measurement of confining pressure. Accordingly, the inner diameter and external diameter of the die were designed as 10 and 20 mm respectively, and the initial height of BSCCO powder was 21.48 mm. All the surfaces of the die and punch were lubricated with a mixture of graphite and vaseline to ensure that the recorded stress states were close to the principal stress conditions.

Compression of the powder materials involves a number of different mechanisms, such as relative particle movement, elastic distortion, plastic deformation and perhaps particle fracture. In contrast, unloading of the powder aggregate is largely an elastic process. Therefore, loading and unloading experiments were carried out to study the elastic and plastic behaviour of the BSCCO powder aggregate.

Loading and unloading experiment

A loading and unloading experiment was performed on BSCCO powder. The initial density of the BSCCO powder was 1.6 g/cm^3 and the strain rate was 3.97×10^{-4} s^{-1}. The curves of axial stress *vs.* axial strain and radial stress versus axial strain are shown in Fig. 5. In this experiment, the compression stress reached 229.93 MPa. So, along the curve AB (loading phase), the densification of powder increased. When the upper punch approached the removable state, the elastic unloading started at point B and progressed linearly until point D. At point D, the punch lost contact with the tablet, hereafter some dilatancy of compact BSCCO powder occurred along DE. Finally, the tablet was free to recover until point E [14].

Cyclic loading and unloading experiment

The cyclic loading and unloading process continued until a pre-selected higher density was reached. The strain rate was about 3.97×10^{-4} s^{-1}. From this experiment, the curves of axial stress versus axial strain and radial stress versus axial strain could be obtained, as shown in Fig. 6.

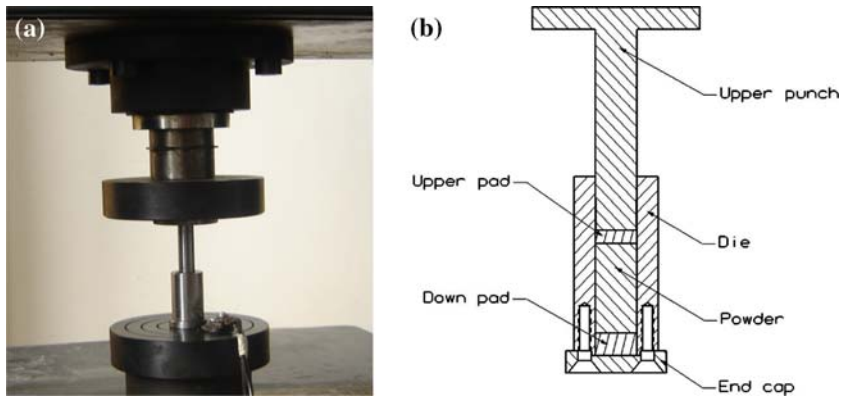

Fig. 4 Experiment of cylindrical die compression with a strain gauge: (**a**) experimental equipment, (**b**) sectional drawing of equipment

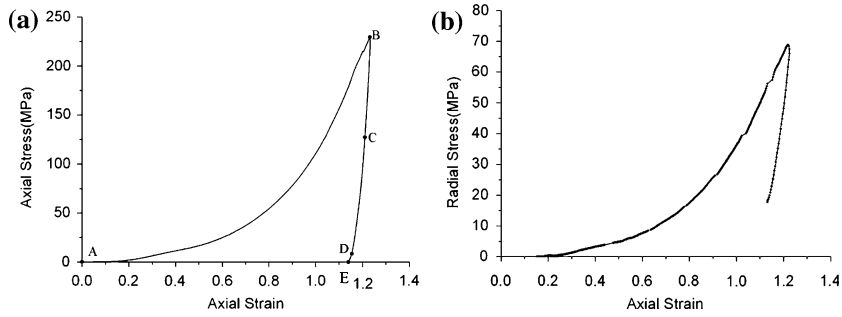

Fig. 5 (**a**) Axial stress versus axial strain, (**b**) radial stress versus axial strain during loading and unloading

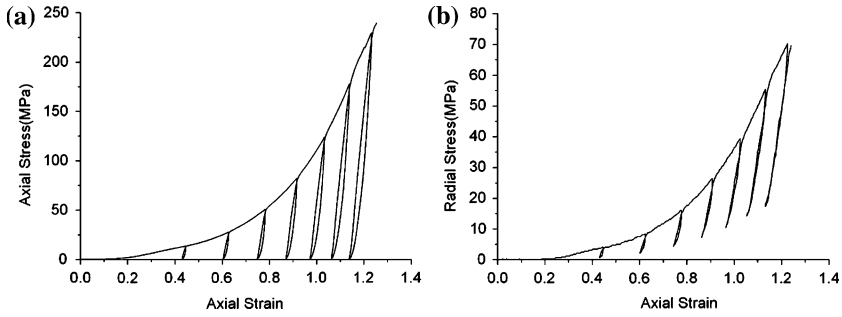

Fig. 6 (**a**) Axial stress versus axial strain, (**b**) radial stress vs. axial strain during cyclic loading and unloading

Experiment of pushing force

During the loading and unloading process, the friction between the BSCCO ceramic powder and cylinder die results in additional axial stress, so it is necessary to eliminate the influence of friction. To investigate the friction between the BSCCO ceramic powder and cylinder die, experiment was also carried out to investigate the friction when the compact powder (powder density was about 4.0 g/cm^3) was pushed though the die. The curve of pushing force versus axial displacement was recorded, as shown in Fig. 7.

Determination of the relation between axial stress and radial stress

The elastic strain of the steel die is slight and negligible during loading and unloading. So the radial stress of BSCCO powder can be computed indirectly from the measurements from strain gauge, and the axial stress of BSCCO powder can be obtained directly from the recorded results of the compressor. The curves of axial stress *vs.* radial stress under different densities during loading and unloading are shown in Fig. 8, respectively.

Figure 8 shows a linear relation between axial stress and radial stress under different densities during loading and unloading when the strain rate is low (3.97×10^{-4} s^{-1}). These linear relations are consistent with [16].

During loading, the ratios of axial stress to radial stress did not differ much under different densities:

$$\gamma = \frac{\sigma_z}{\sigma_r} = 3.08 \tag{9}$$

During unloading, a linear relation between axial stress and radial stress can be written as:

$$\sigma_z = a\sigma_r - b(\rho) \tag{10}$$

where a is the slope and b is the residual radial stress.

From Fig. 8b, the slopes were almost same at different densities, $a = 5.62$. Residual radial stress b is a function of density, $b(\rho) = 5.42\rho - 12.9$ MPa, as shown in Fig. 9.

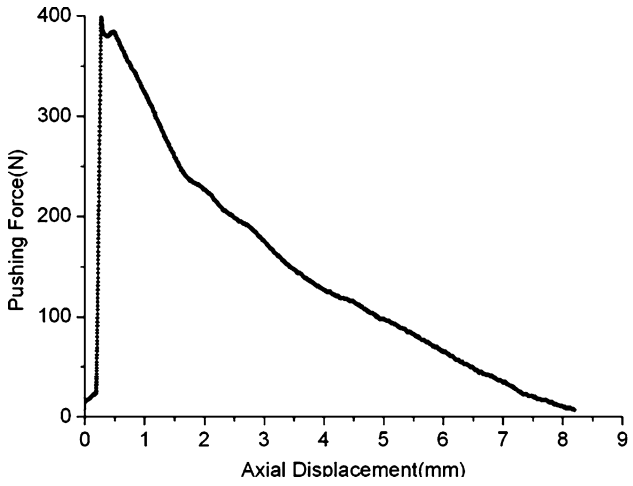

Fig. 7 Pushing force versus axial displacement during pushing out of BSCCO powder

The coefficient of friction μ between the compact BSCCO powder and the die

The curve of pushing force, shown in Fig. 7, comprises two phases, and the peak of the curve is their dividing point. During the first phase, the pushing force is smaller than the friction force, the compact cylinder of BSCCO powder does not move, and the pushing force increases sharply until reaching a peak, which results in extra radial stress. The extra radial stress can be computed by using the relation between axial stress and radial stress during loading, $\sigma_r^{extra} = \frac{\sigma_z}{3.08} = 1.65$ MPa.

The second phase indicates that the compact cylinder of BSCCO powder begins moving. The pushing force is mainly used to overcome the friction between BSCCO powder and the die. As the contact surface between the compact cylinder of BSCCO powder and the die decreases, the pushing force decreases gradually.

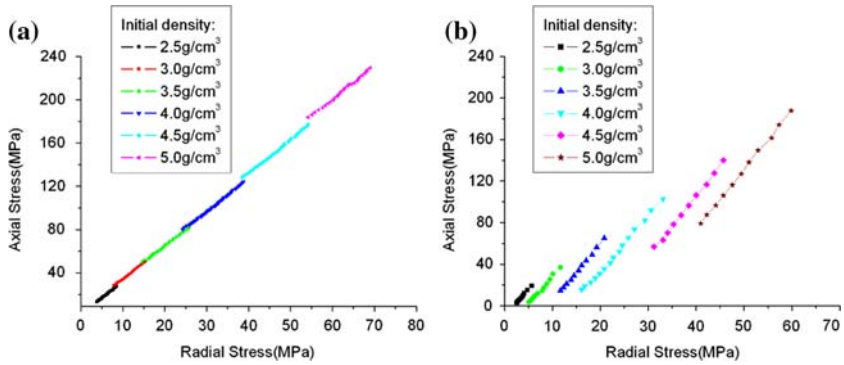

Fig. 8 Axial stress versus axial strain under different densities during loading (**a**), and during unloading (**b**)

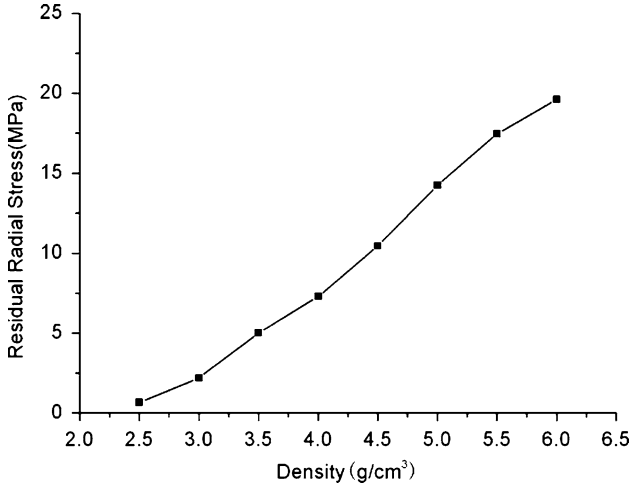

Fig. 9 Residual radial stress versus density during unloading

The peak of the curve is the critical force to overcome the friction between the compact cylinder of BSCCO powder and the die. According to force equilibrium, $\pi Dh\mu\sigma_{\mathrm{r}} = \pi Dh\mu(\sigma_{\mathrm{r}}^{\mathrm{extra}} + \sigma_{\mathrm{r}}^{\mathrm{res}})$, where $\sigma_{\mathrm{r}}^{\mathrm{res}} = 6.93\,\mathrm{MPa}$. The coefficient of friction $\mu = 0.176$ can be obtained. This coefficient of friction was computed under a lubrication situation in which there was a mixture of graphite and vaseline between the BSCCO powder and the die.

Calibration of constitutive model of BSCCO powder

Elastic parameters

The cyclic loading-unloading-reloading responses are shown in Fig. 6. Plastic deformation is apparent as the non-linear behaviour at very low loads. However, both the unloading curves and reloading curves have parallel linear portions consistent with elastic deformation over the in-between range. So the elastic parameters can be calculated from the linear portions of the unloading curves at the prevailing density by using the linear elastic theory [17]. In cylindrical closed die compression, the circumferential stress σ_θ is assumed to be equal to the radial stress σ_{r}, and this assumption is also applicable in the consequent computation. The general Hooke's law can be written as

$$\varepsilon_z = \frac{1}{E}(\sigma_z - 2v\sigma_{\mathrm{r}}) \tag{11}$$

$$\varepsilon_{\mathrm{r}} = \frac{1}{E}[(1-v)\sigma_{\mathrm{r}} - v\sigma_z] \tag{12}$$

where E and v are the Young's modulus and Poisson's ratio of the compact BSCCO powder, σ_z andσ_{r} are the axial stress and radial stress, and ε_z and ε_{r} are the axial strain and radial strain. The Young's modulus and Poisson's ratio can be computed as follows:

$$v = \frac{\Delta\sigma_z\Delta\varepsilon_{\mathrm{r}} - \Delta\sigma_{\mathrm{r}}\Delta\varepsilon_z}{2\Delta\sigma_{\mathrm{r}}\Delta\varepsilon_{\mathrm{r}} - (\Delta\sigma_z + \Delta\sigma_{\mathrm{r}})\Delta\varepsilon_z} \tag{13}$$

$$E = \frac{\Delta\sigma_z - 2v\Delta\sigma_{\mathrm{r}}}{\Delta\varepsilon_z}. \tag{14}$$

The computational results of Young's modulus E and Poisson's ratio v are shown in Fig. 10. The Young's modulus E increases exponentially with the increase of relative density. It is important to note that the values of Young's modulus are extremely small especially in the low-density area. In fact, it is known that no elasticity is presented in the compression of loose metal powders, whereas high-density compacts behave elastically in a way that is similar to wrought materials. This computational result is close to the result in [10], in which the Young's modulus E was measured by using an ultrasound wave propagation technique. After fitting of these data, the relation between the Young's modulus E and the relative density of BSCCO powder can be written as

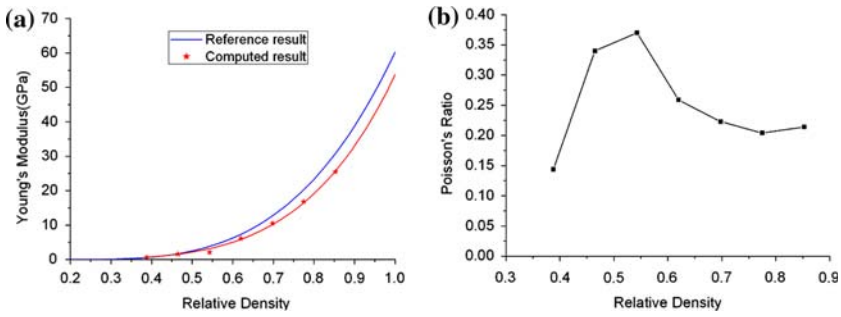

Fig. 10 Elastic parameters: (**a**) Young's modulus versus relative density, (**b**) Poisson's ratio versus relative density

$$E = 53.754\rho_r^{4.6}\ \text{GPa} \tag{15}$$

where ρ_r is the relative density. However, the Poisson's ratio v increases with the increase of relative density until the relative density reaches to 0.55 at which point the Poisson's ratio v begins decreasing. This phenomenon possibly results from the rearrangement of powder particles, which marks the transition from phase 1 behaviour (in which the interparticle force and localized plastic deformation is dominant) to phase 2 behaviour (in which the bulk plastic deformation is dominant). Rearrangement of powder particles has an effect mostly on the ratio of axial to transverse properties of the powder compact [18]. This tendency is different from the result of [10].

Other parameters

In the cylindrical closed die compression, the circumferential stress is assumed to be equal to the radial stress, the hydrostatic pressure and the second invariant of deviatoric stress tensor can be written as follows:

$$p = \frac{1}{3}(\sigma_z + 2\sigma_r) \quad \text{and} \quad \sqrt{J_2'} = \frac{1}{\sqrt{3}}|\sigma_z - \sigma_r|$$

The procedure used for computing model parameters is based on the stress path for the cap model of the confined compression experiment. From Fig. 5, the stress path of the confined compression experiment on the $p - \sqrt{J_2'}$ plane can be obtained, as shown in Fig. 11.

During the loading phase, the stress path $(p, \sqrt{J_2'})$ of BSCCO powder is a straight line AB starting from (0,0) and intersecting the cap ($F_c(p, \sqrt{J_2'}) = 0$) at point B. Then the stress path during unloading follows the line BC until $\sqrt{J_2'} = 0$. At point C, the stress state is hydrostatic ($\sigma_z = \sigma_r$). After point C, the radial stress is greater than the axial stress. Since the modulus $\sqrt{J_2'}$ is positive, the elastic path continues with increasing $\sqrt{J_2'}$ until it intersects the failure surface $F_s(p, \sqrt{J_2'}) = 0$ at D. Hereafter, plastic deformation occurs from D to E, and DE is parallel to AB. The slopes of BC and CD lines are equal to $\frac{2G}{\sqrt{3}K}$, where K is the compressibility and G is the shear modulus [13].

From Fig. 11, the values of the second invariant of deviatoric stress tensor $\sqrt{J_2'}$ and the hydrostatic stress P at points A, B, C, D and E are summarized in Table 1.

Computing the internal angle of friction β

As presented in the stress path diagram, Fig. 11, the internal angle of friction β is defined as the slope angle of line AB. From the experimental data of BSCCO powder summarized in Table 1, we can obtain $\tan\beta = \frac{\sqrt{J_2'(B)}}{p(B)} = 0.742$, so the internal angle of friction β is equal to 36.6°.

Computing cohesion d

Since D is on the F_s surface, cohesion d can be computed by the following equation:

$$d = \sqrt{J_2'(D)} - p(D)\tan\beta. \tag{16}$$

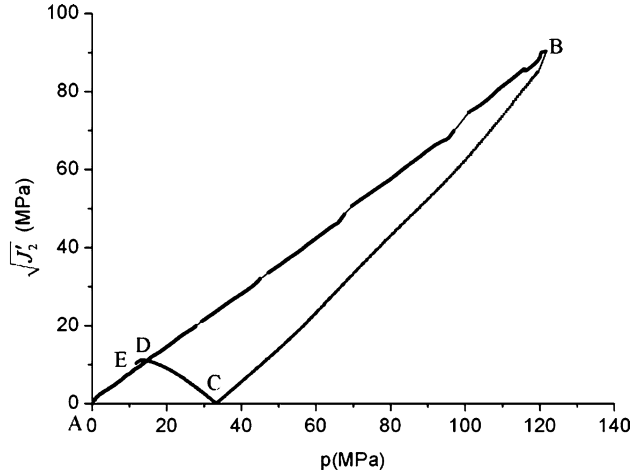

Fig. 11 Stress path of the confined compression experiment on the $p - \sqrt{J_2'}$ plane

Table 1 Experimental data of BSCCO powder

	A	B	C	D	E
$\sqrt{J_2'}$ (MPa)	0	90.38	0	11.12	10.27
p (MPa)	0	121.78	33.43	13.23	11.86

Table 2 The computed parameters of constitutive model of BSCCO powder

Young's modulus, E	$E = 53.754\rho_r^{4.632}$ (GPa)
Internal angle of friction, β	36.6°
Cohesion, d	1.30 MPa
Coefficient of friction between BSCCO and die, μ	0.176
Transition surface parameter, α	0.05

So, the resulting cohesion d of BSCCO powder is estimated to be 1.3 MPa.

The computed parameters of the constitutive model of BSCCO powder are summarized in Table 2.

Simulation of the confined compression test for BSCCO powder

In order to verify the feasibility of the computed parameters in the constitutive model for BSCCO powder, the confined compression test was analysed numerically. The density of BSCCO powder before compression was about 2.5 g/cm^3, and other material parameters are listed in Table 3.

A commercial finite element program, ABAQUS, was adopted for the numerical modelling, and the explicit and dynamic calculation method was applied. The dimension of the simulated powder was same as the experiment sample: R = 5 mm, h = 13.75 mm. Due to the axial symmetry, the compacted powder was meshed with 128 four-node axisymmetric stress elements (CAX4R) as shown in Fig. 12. During the compression, the coefficient of friction between the BSCCO powder and the die is 0.176. Figure 13 showed the von Mises stress contours when the powder was compacted up to 50% of deformation.

Table 3 Material parameters of BSCCO powder

Young's modulus, E	626 MPa
Poisson's ratio, v	0.14
Internal angle of friction, β	36.6°
Cohesion, d	1.30 MPa
Eccentricity, R	0.29
Transition surface parameter, α	0.05
Coefficient of friction between BSCCO and die, μ	0.176

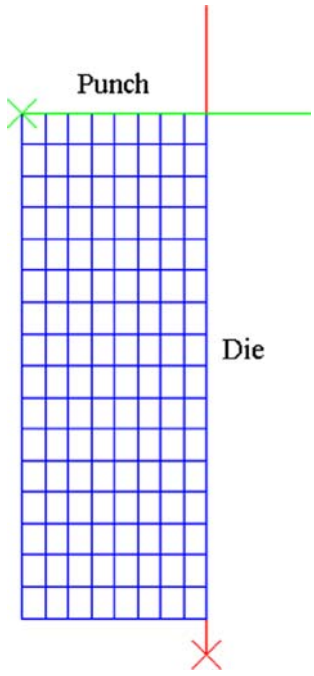

Fig. 12 Undeformed mesh of BSCCO powder (axisymmetric)

The experimental and the simulated curves of axial stress versus axial strain were shown in Fig. 14. The simulated results agreed with experiment on the whole. However, we can find that the difference between the experimental and the simulated stress became larger

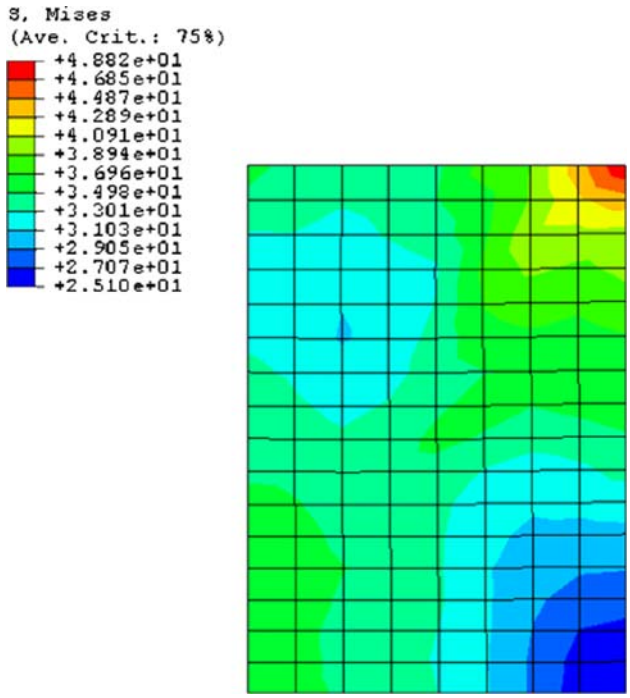

Fig. 13 The von Mises stress contour when the powder was compacted up to 50% of deformation

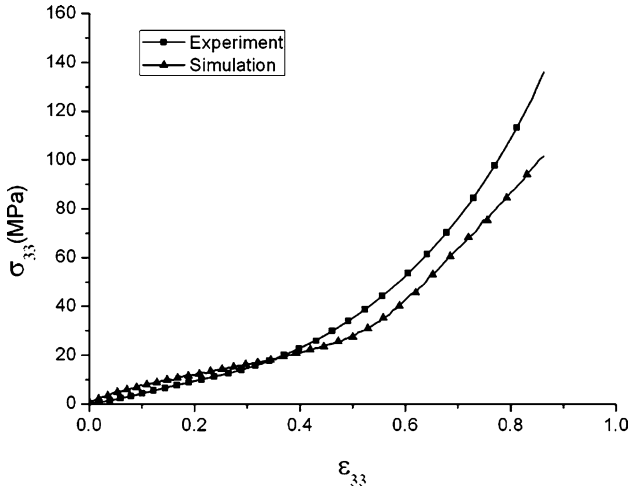

Fig. 14 Stress versus strain of experiment and simulation in confined compression

and larger with the increase of the strain. The main reason of this phenomenon was that the powder particle size is very small, with the increase of deformation, and more and more particles were filled in the gap between the die and the punch. Therefore, the friction between the die and the punch increased, which led to additional stress. But this effect was not considered in the numerical simulation.

Conclusions

The modified Drucker–Prager/Cap model was proposed to describe the constitutive behaviour of BSCCO powder during compression. Compared with other related research, the present modified model needs only a hydrostatic experiment and cyclic loading-unloading experiments.

An associated methodology was performed to calculate the parameters of the constitutive model with the experimental data of cyclic loading and unloading, which confirms that there is a linear relation between radial stress and axial stress during loading and unloading when the strain rate is low. According to force equilibrium, the friction coefficient between BSCCO powder and the die was estimated from the pushing-out experiments.

The modified Drucker–Prager/Cap model was used to simulate the confined compression of the BSCCO powder. The numerical results were closed to the experimental results, which verified the reliability of this constitutive model. Based on this constitutive model of BSCCO powder, further simulation for the manufacture of superconducting Bi–2223/Ag tapes can be developed.

Acknowledgement This research has been carried out under the projects 50575124 and 50305015 supported by National Natural Science Foundation of China.

References

1. Yi HP, Han Z, Zhang JS, Liu T, Liu L, Li MY, Fang J, Liu Q, Zheng YK (2004) Physica C 412–414:1073
2. Oliver J, Oller S, Cante JC (1996) Int J Solids Struct 33:3161
3. Turner CD (1994) Proc 1994 Powder Metall World Congr 713
4. Skisaya AR, Cocks ACF, Fleck NA (1994) Proc 1994 Powder Metall World Congr 757
5. Ransing RS, Gethin DT, Khoei AR, Mosbah P, Lewis RW (2000) Mater Design 21:263
6. Martin CL, Bouvard D (2003) Acta Mater 51:373
7. ABAQUS Inc. (2003) ABAQUS Analysis User's Manual
8. Drucker DC, Prager W (1952) Q Appl Math 10:157
9. Suh NP (1969) Int J Powder Metall 5:69
10. Gurson AL, Yuan DW (1995) Net Shape Process Powder Mater AMD 216:57
11. Bech JI, Eriken M, Toussaint F, Doremus P, Bay N (2000) Proc 2000 Powder Metall World Congr 1453
12. Allais A, Bruzek CE, Montmitonnet P, Herrmann P, Pelissier D, Toussaint F (2003) IEEE Trans Appl Supercond 13:3026
13. Michrafy A, Ringenbacher D, Tchoreloff P (2002) Powder Technol 127:257
14. Aydin I, Briscoe BJ, Sanliturk KY (1996) Powder Technol 89:239
15. Chtourou H, Guillot M, Gakwaya A (2002) Int J Solids Struct 39:1059
16. Es and Saheb MH (1992) J Mater Sci 27:4151
17. Carnavas PC, Page NW (1998) J Mater Sci 33:4647
18. Martin CL (2004) J Mech Phys Solids 52:1691